Wireless Power Transfer to Miniature Implants: Transmitter Optimization

Sanghoek Kim, *Student Member, IEEE*, John S. Ho, *Student Member, IEEE*, and Ada S. Y. Poon, *Senior Member, IEEE*

***Abstract*—This paper examines transmitter optimization for wirelessly powering a small implant embedded in tissue. The wireless link between the transmitter and receiver is first modeled as a two-port network and an expression for the power transfer efficiency derived. For a given small receiver in a multilayer tissue model, the transmitter is abstracted as a sheet of magnetic current density for which the optimal distribution is analytically found. The optimal transmitter is compared to the point and uniform source across a range of frequencies. At higher frequencies, the optimal current distribution is shown to induce fields that exhibit focusing. The effects of constructive and destructive interference substantially improves the power transfer efficiency and reinforces operation in the low GHz-range. The optimal transmitter establishes an upper bound on the power transfer efficiency for a given implant and provides insight on the design of the optimal transmit antenna.**

***Index Terms*—Wireless power transfer, wireless implant, near-field antenna, layered media, SAR, power transfer efficiency.**

I. Introduction

Implantable medical devices for sensing, drug delivery, and local stimulation will play an increasingly important role in modern medicine. These devices help manage a broad range of medical disorders through preventive and post-surgery monitoring. In order to avoid the risks associated with battery replacement and enable miniaturization of the implant, wireless delivery of energy to these devices is desirable. Traditionally, researchers have operated at sufficiently low frequencies ($<$ 10 MHz) such that tissue absorption is negligible. Safety regulations that limit heating of tissue were thus not included in most studies [1–5]. Recently, it was shown that the optimal frequency for wireless power transfer lies in the sub-GHz to the low GHz-range [6]. The analysis in [6] used point sources to model both the transmit and the receive antennas, and derived an expression for the optimal frequency of power transmission by modeling tissue as a homogeneous medium. Using a more complex model consisting of planar tissue layers, it was numerically shown that the optimal frequency remains in the sub-GHz to the low-GHz region.

At low frequencies, most transmitted energy is stored in fields rather than radiated. The wireless link between the transmitter and receiver can thus be analyzed in terms of inductive coupling. Under these conditions, the coil is a natural choice of transmit structure; most analyses based on inductive coupling are concerned with the design of a coil. Since the wavelength is much longer than the distance between the transmitter and receiver, further optimization is unnecessary since changes in the structure do not result in significantly different field distributions in tissue. At higher frequencies, however, the wavelength is comparable to the distance of separation. As a result of interference, the fields can be redistributed in tissue by the appropriate choice of transmitter. Optimizing the transmitter for power transfer efficiency can enable significantly greater power delivery while avoiding excessive heating of tissue.

We consider the problem of finding the optimal transmitter for a small receiver in tissue. Given the greater degree of freedom allowed in the design of the external transmit antenna, [7] removed restrictions on the dimension and structure of transmit antenna by modeling the transmitter as an infinite sheet of magnetic current density. The distribution maximizing the power transfer efficiency was analytically solved for a receive magnetic dipole oriented along the z direction and air-tissue inhomogeneity modeled as a planarly half-space medium. In this work, we generalize the analysis in [7]. We consider a multilayer tissue model and allow for a small receiver modeled as a combination of an electric and magnetic dipoles of arbitrary orientation for completeness. By finding the optimal current distribution, an upper limit on power transfer efficiency for a magnetic current distribution can be established for a given implant in tissue.

The rest of the paper is organized as follows. Section II presents the source and the tissue models as well as the expression for the *coupling parameter*. Section III expresses the coupling parameter in terms of the transmit current distribution. Section IV derives the optimal current distribution that maximizes the coupling parameter. Section V compares the performance of optimal source to that of a point source and a uniform source, and shows the resulting field distributions in tissue as well as the properties of the optimal transmitter. Section VI discusses receiver considerations and relates the optimization gain to power transfer efficiency. Finally, we conclude this paper in Section VII.

In this paper, we will use boldface letters for vectors and boldface capital letters with a bar such as $\bar{\mathbf{G}}$ for matrices. For a complex number x, $\mathrm{Re}\, x$ and $\mathrm{Im}\, x$ denote the real and imaginary part of x respectively. For a vector $\mathbf{r}$, r denotes its magnitude and $\hat{\mathbf{r}}$ is a unit vector denoting its direction. $(\cdot)^*$ and $(\cdot)^t$ denote the conjugate and transpose operations respectively.

The material in this paper was presented in part at the International Symposium On Antennas and Propagation and USNC/USRI National Radio Science Meeting, July 2011.

S. Kim, J. S. Ho, and A. S. Y. Poon are with the Department of Electrical Engineering, Stanford University, 94305, USA (e-mail:kshyuk@stanford.edu; johnho@stanford.edu; adapoon@stanford.edu).

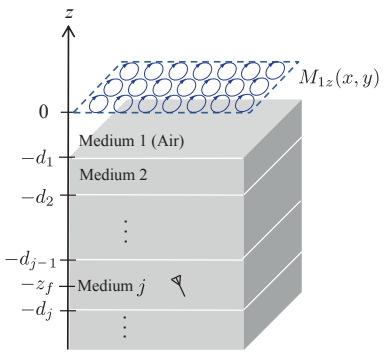

Figure 1. A planar current source $M_{1z}(x,y)$ on top of a multilayer inhomogeneous tissue model delivers power to an implanted antenna at $z=-z_f$.

II. Model and Problem Formulation

A. Source and Tissue Models

We model the inhomogeneity of the link as an air-tissue planarly multilayered medium, as illustrated in Fig. 1. The transmit antenna is modeled as an infinite sheet of magnetic current density at $z=0$ with distribution

$$\mathbf{M}_1(\mathbf{r}) = M_{1z}(x,y)\,\delta(z)\,\hat{\mathbf{z}}. \tag{1}$$

Since the receive antenna is small, it can be modeled as a combination of magnetic and electric dipoles with arbitrary orientation located at $\mathbf{r}=\mathbf{r}_f$:

$$\mathbf{M}_2(\mathbf{r}) = i\omega\mu A_r I_2\,\delta(x,y,z+z_f)\,\boldsymbol{\alpha} \tag{2a}$$
$$\mathbf{J}_2(\mathbf{r}) = l_r I_2\,\delta(x,y,z+z_f)\,\boldsymbol{\beta} \tag{2b}$$

where A_r is the area of the magnetic dipole and $A_r I_2$ is its magnetic moment, and l_r is the length of the electric dipole and $l_r I_2$ is its electric moment. The vectors $\hat{\boldsymbol{\alpha}}$ and $\hat{\boldsymbol{\beta}}$ denote the orientation of the magnetic and electric dipoles respectively, and the relative contributions from the two dipoles are normalized such that $\alpha^2+\beta^2=1$. For a given $\mathbf{M}_2$ and $\mathbf{J}_2$, we want to find $M_{1z}(x,y)$ that optimizes the power transfer efficiency, as will be next defined.

B. Coupling Parameter

Fig. 2 shows a typical wireless power transfer system. In this work, we focus on the power transfer efficiency over the transmission link shown as the shaded region of Fig. 2. The coupling between the transmit and the receive structures can be abstracted as a two-port network:

$$V_1 = Z_{11}I_1 + Z_{12}I_2$$
$$V_2 = Z_{21}I_1 + Z_{22}I_2.$$

Denoting the equivalent input impedance of the power receiver as Z_L, we have $V_2=-Z_L I_2$ and hence,

$$I_2 = -\frac{Z_{21}}{Z_{22}+Z_L} I_1.$$

Now, the received power at the output of the two-port network can be written as

$$P_r = R_L\left|I_2\right|^2 \tag{3}$$

where R_L is the real part of Z_L. Since receive structure is small, the transmitter and receiver are *loosely coupled*. The transmit power at the input of the two-port network can then be approximated by

$$P_t = \mathrm{Re}\{V_1 I_1^*\} \approx R_{11}\left|I_1\right|^2. \tag{4}$$

where R_{11} is the real part of Z_{11}. The power transfer efficiency is thus given by

$$\eta := \frac{P_r}{P_t} \approx \frac{\left|Z_{21}\right|^2}{4R_{11}R_{22}} \frac{4R_{22}R_L}{\left|Z_{22}+Z_L\right|^2}. \tag{5}$$

In this expression, the efficiency is the product of two factors: the *coupling efficiency* η_c on the left and the *matching efficiency* η_m on the right. The coupling efficiency is the ratio of the power available at the receiver to the input power. The matching efficiency is the ratio of the power delivered to the load to the available power. In this paper, we focus on optimizing the transmitter for a given receiver. Since the matching efficiency is independent of the transmit structure, it suffices to maximize the coupling efficiency. From η_c, we extract the *coupling parameter* γ

$$\gamma = \frac{|Z_{21}|^2}{R_{11}}, \tag{6}$$

which is completely determined by the transmitter. The optimal transmitter is thus given by the current distribution $M_{1z}(x,y)$ that maximizes γ.

III. Self and Mutual Impedances

To maximize the coupling parameter for a given receiver, we will need to express the coupling parameter in terms of $M_{1z}(x,y)$ first. This is achieved by first defining the impedances of the two-port network in terms of the electromagnetic fields from the sources $\mathbf{M}_1$, $\mathbf{M}_2$, and $\mathbf{J}_2$. We then derive these fields in terms of the source distributions.

A. Definitions

For a loosely coupled two-port network, the real part of Z_{11} accounts for the tissue loss, the conduction loss in the transmit structure, and the radiation loss. Tissue loss usually dominates the radiation loss, since the radiation efficiency is poor due to the presence of lossy tissue in near-field region. We assume that the antenna efficiency is close to unity. Denoting the electric and the magnetic fields from the transmit source by $\mathbf{E}_1(\mathbf{r})$ and $\mathbf{H}_1(\mathbf{r})$ respectively,

$$R_{11} = \frac{\omega}{\left|I_1\right|^2}\int_{z<-d_1} \mathrm{Im}\,\epsilon(\mathbf{r})\left|\mathbf{E}_1(\mathbf{r})\right|^2 d\mathbf{r} \tag{7}$$

where $\epsilon(\mathbf{r})$ is the permittivity at $\mathbf{r}$.

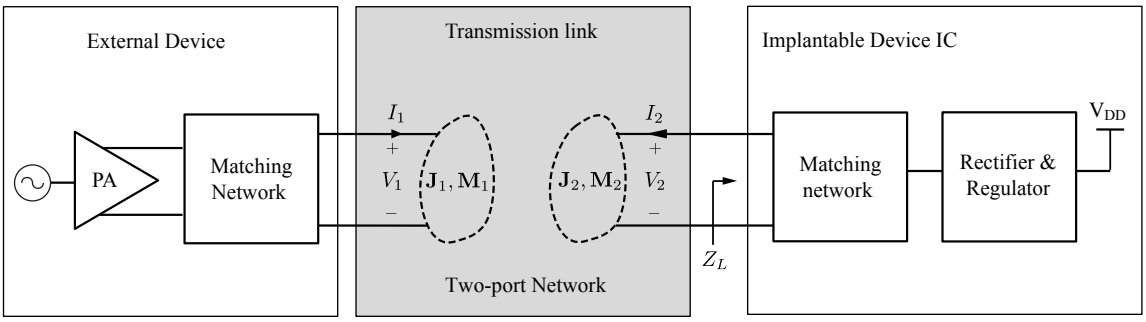

Figure 2. Overall wireless power transfer system. This work focuses on the analysis and the optimization of the shaded region. $(\mathbf{J}_1, \mathbf{M}_1)$ are the electric and the magnetic current distributions on the external antenna structure while $(\mathbf{J}_2, \mathbf{M}_2)$ are those on the implant antenna structure.

We define the mutual impedance via the concept of induced emf [8, Chapter 3]. It is given by

$$Z_{21} = \frac{1}{I_1 I_2}\left(\int \mathbf{M}_2 \cdot \mathbf{H}_1 \, d\mathbf{r} + \int \mathbf{J}_2 \cdot \mathbf{E}_1 \, d\mathbf{r}\right) \tag{8a}$$

$$= \frac{V_{oc}}{I_1}, \tag{8b}$$

where V_{oc} is the received open circuit voltage of

$$V_{oc} = i\omega\mu A_r \, \boldsymbol{\alpha} \cdot \mathbf{H}_1(\mathbf{r}_f) + l_r \, \boldsymbol{\beta} \cdot \mathbf{E}_1(\mathbf{r}_f) \tag{9}$$

for a small receive dipole. Putting these together,

$$\gamma = \frac{\left| i\omega\mu A_r \, \boldsymbol{\alpha} \cdot \mathbf{H}_1(\mathbf{r}_f) + l_r \, \boldsymbol{\beta} \cdot \mathbf{E}_1(\mathbf{r}_f) \right|^2}{\omega \int_{z<-d_1} \operatorname{Im} \epsilon(\mathbf{r}) \left|\mathbf{E}_1(\mathbf{r})\right|^2 d\mathbf{r}}. \tag{10}$$

B. Expressions for the Fields

The electromagnetic fields can be expressed in terms of source through the Green's functions:

$$\mathbf{H}_1(\mathbf{r}) = i\omega\epsilon \int \bar{\mathbf{G}}_{hm}(\mathbf{r} - \mathbf{r}') \mathbf{M}_1(\mathbf{r}') \, d\mathbf{r}' \tag{11a}$$

$$\mathbf{E}_1(\mathbf{r}) = -\int \bar{\mathbf{G}}_{em}(\mathbf{r} - \mathbf{r}') \mathbf{M}_1(\mathbf{r}') \, d\mathbf{r}. \tag{11b}$$

Taking the 2D Fourier transform with respect to (x, y) for a given depth z yields

$$\mathcal{H}_1(k_x, k_y, z) = i\omega\epsilon \, \bar{\mathfrak{G}}_{hm}(k_x, k_y, z) \hat{\mathbf{z}} \, \mathcal{M}_{1z}(k_x, k_y) \tag{12a}$$

$$\mathcal{E}_1(k_x, k_y, z) = -\bar{\mathfrak{G}}_{em}(k_x, k_y, z) \hat{\mathbf{z}} \, \mathcal{M}_{1z}(k_x, k_y). \tag{12b}$$

In free-space, via the use of Weyl identity, the Green's functions are given by

$$\bar{\mathfrak{G}}_{hm,fs}(k_x, k_y, z) = \frac{ie^{-ik_z z}}{2k_z}\left(\bar{\mathbf{I}} - \frac{\mathbf{k}\mathbf{k}^t}{k^2}\right)$$

$$\bar{\mathfrak{G}}_{em,fs}(k_x, k_y, z) = -\frac{e^{-ik_z z}}{2k_z} \mathbf{k} \times \bar{\mathbf{I}}$$

where $k_z = \sqrt{k^2 - k_x^2 - k_y^2}$, $\mathbf{k} = \begin{bmatrix} k_x & k_y & -k_z \end{bmatrix}^t$, and k is the wavenumber of free-space. In the multi-layered medium, we need to include the reflection and the transmission coefficients. From [9, Chapter 2], when z is in between $-d_{n+1}$ and $-d_n$, the Green's functions can be written as

$$\bar{\mathfrak{G}}_{hm,n}(k_x, k_y, z) = \frac{i}{2k_{1z}}\left(\bar{\mathbf{I}} - \frac{\mathbf{k}_1 \mathbf{k}_1^t}{k_1^2}\right) \cdot A_n \left[e^{-ik_{nz}z} + \tilde{R}^{TE}_{n,n+1} e^{ik_{nz}(z+2d_n)}\right] \tag{13a}$$

$$\bar{\mathfrak{G}}_{em,n}(k_x, k_y, z) = -\frac{1}{2k_{1z}} \mathbf{k}_1 \times \bar{\mathbf{I}} \cdot A_n \left[e^{-ik_{nz}z} + \tilde{R}^{TE}_{n,n+1} e^{ik_{nz}(z+2d_n)}\right] \tag{13b}$$

where $k_{nz} = \sqrt{k_n^2 - k_x^2 - k_y^2}$, $\mathbf{k}_n = \begin{bmatrix} k_x & k_y & -k_{nz} \end{bmatrix}^t$, and k_n is the wavenumber of the nth layer. The term $\tilde{R}^{TE}_{n,n+1}$ is the generalized reflection coefficient while A_n can be interpreted as the generalized transmission coefficient. Their expressions can be found in [9, Chapter 2]. Once $\mathcal{M}_{1z}(k_x, k_y)$ is known, performing the inverse Fourier transform yields the electromagnetic fields at any point in space.

IV. Optimal Transmit Current Distribution

We will now express the coupling parameter in (10) in terms of $\mathcal{M}_{1z}(k_x, k_y)$. For a Fourier transform pair $g(t)$ and $G(\omega)$, $g(0) = \frac{1}{2\pi}\int G(\omega) \, d\omega$. Therefore,

$$\mathbf{H}_1(0, 0, -z_f) = \frac{1}{4\pi^2} \iint \mathcal{H}_1(k_x, k_y, -z_f) \, dk_x dk_y \tag{14}$$

and hence,

$$\mathbf{H}_1(0, 0, -z_f) = \frac{i\omega\epsilon_1}{4\pi^2} \iint \bar{\mathfrak{G}}_{hm,j}(k_x, k_y, -z_f) \hat{\mathbf{z}} \, \mathcal{M}_{1z}(k_x, k_y) \, dk_x dk_y. \tag{15}$$

Similarly,

$$\mathbf{E}_1(0, 0, -z_f) = -\frac{1}{4\pi^2} \iint \bar{\mathfrak{G}}_{em,j}(k_x, k_y, -z_f) \hat{\mathbf{z}} \, \mathcal{M}_{1z}(k_x, k_y) \, dk_x dk_y. \tag{16}$$

By Parseval's theorem, $\int |g(t)|^2\, dt = \frac{1}{2\pi}\int |G(\omega)|^2\, d\omega$. Therefore,

$$\begin{aligned}
&\int_{z<-d_1} \operatorname{Im}\epsilon(z)\left|\mathbf{E}_1(\mathbf{r})\right|^2 d\mathbf{r} \\
=&\frac{1}{4\pi^2}\iiint_{z<-d_1} \operatorname{Im}\epsilon(z)\left|\boldsymbol{\mathcal{E}}_1(k_x,k_y,z)\right|^2 dk_x dk_y dz \quad (17a)\\
=&\frac{1}{4\pi^2}\iint\Big[\int_{z<-d_1} \operatorname{Im}\epsilon(z)\left|\bar{\mathfrak{G}}_{em}(k_x,k_y,z)\hat{\mathbf{z}}\right|^2 dz\Big] \quad (17b)\\
&\cdot\left|\mathcal{M}_{1z}(k_x,k_y)\right|^2 dk_x dk_y.
\end{aligned}$$

Defining

$$\begin{aligned}
h(k_x,k_y) &= \frac{1}{4\pi^2}\Big[k_1^2 A_r \boldsymbol{\alpha}^t \bar{\mathfrak{G}}_{hm,j}(k_x,k_y,-z_f)\hat{\mathbf{z}} \\
&\qquad + l_r \boldsymbol{\beta}^t \bar{\mathfrak{G}}_{em,j}(k_x,k_y,-z_f)\hat{\mathbf{z}}\Big] \\
f(k_x,k_y) &= \sqrt{\frac{\omega}{4\pi^2}\int_{z<-d_1} \operatorname{Im}\epsilon(\mathbf{r})\left|\bar{\mathfrak{G}}_{em}(k_x,k_y,z)\hat{\mathbf{z}}\right|^2 dz},
\end{aligned}$$

the coupling parameter in (10) can be written as

$$\gamma = \frac{\left|\iint h(k_x,k_y)\mathcal{M}_{1z}(k_x,k_y)\, dk_x dk_y\right|^2}{\iint\left|f(k_x,k_y)\mathcal{M}_{1z}(k_x,k_y)\right|^2 dk_x dk_y}. \quad (18)$$

The optimization problem is to find $\mathcal{M}_{1z}(k_x,k_y)$ such that the expression in (18) is maximized. By the Cauchy-Schwarz inequality, (18) is maximized when

$$\mathcal{M}_{1z,opt}(k_x,k_y) = \frac{h^*(k_x,k_y)}{\left|f(k_x,k_y)\right|^2} \quad (19)$$

and the optimal value for the coupling parameter in (18) is

$$\gamma_{opt} = \iint\Big|\frac{h(k_x,k_y)}{f(k_x,k_y)}\Big|^2 dk_x dk_y. \quad (20)$$

For example, in a half-space medium, when the receiver is a magnetic dipole oriented along the z direction ($\boldsymbol{\alpha} = \hat{\mathbf{z}}$ and $\boldsymbol{\beta} = \mathbf{0}$), the optimal source distribution is given by

$$\mathcal{M}_{1z,opt}(k_x,k_y) = \frac{A_r(k_{1z}+k_{2z})\operatorname{Im}k_{2z}e^{ik_{2z}^*(-z_f+d_1)}}{2\pi^2\omega e^{ik_{1z}d_1}} \quad (21)$$

and the corresponding coupling parameter in (18) is

$$\gamma_{opt} = \frac{A_r^2}{\pi\omega\operatorname{Im}\epsilon_2}\int_0^\infty \operatorname{Im}k_{2z}e^{2\operatorname{Im}k_{2z}(-z_f+d_1)}k_\rho^3\, dk_\rho \quad (22)$$

where $k_\rho = \sqrt{k_x^2+k_y^2}$. As another example, when the receiver is an electric dipole oriented along the x direction ($\boldsymbol{\alpha} = \mathbf{0}$ and $\boldsymbol{\beta} = \hat{\mathbf{x}}$), the optimal source distribution is given by

$$\mathcal{M}_{1z,opt}(k_x,k_y) = \frac{l_r k_y(k_{1z}+k_{2z})\operatorname{Im}k_{2z}e^{ik_{2z}^*(-z_f+d_1)}}{4\pi^2\omega k_\rho^2 e^{ik_{1z}d_1}} \quad (23)$$

and the corresponding coupling parameter is

$$\gamma_{opt} = \frac{l_r^2}{2\pi\omega\operatorname{Im}\epsilon_2}\int_0^\infty \operatorname{Im}k_{2z}e^{2\operatorname{Im}k_{2z}(-z_f+d_1)}k_\rho dk_\rho. \quad (24)$$

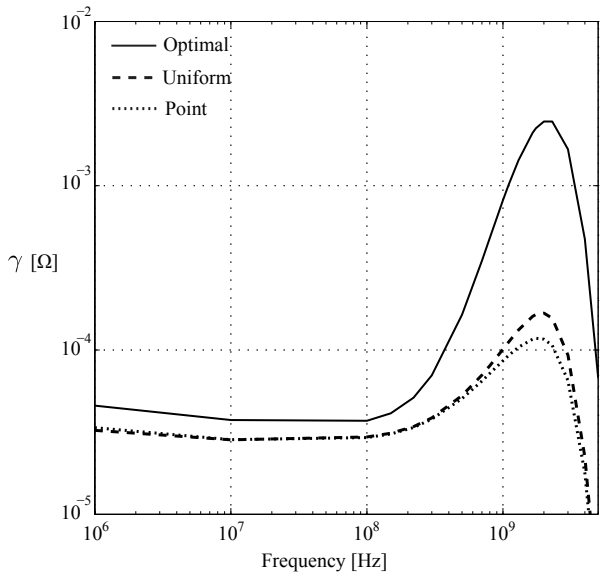

Figure 3. Coupling parameter versus frequency for a vertical magnetic dipole at $z_f = 5$ cm for different source distributions $d_1 = 1$ cm above the interface.

V. Results

A. Comparison with Point and Uniform Sources

We compare the optimal transmit current distribution to a point source and an uniform source in terms of the resulting coupling parameter and field distributions in tissue. The receiver and tissue model must be fixed in order to perform a comparison. For simplicity, we consider a magnetic dipole with an area of $A_r = \pi$ mm^2 oriented in the z direction. For a vertical magnetic dipole receiver, the received open-circuit voltage is given by

$$V_{oc} = i\omega\mu A_r |H_{1z}(\mathbf{r}_f)| \quad (25)$$

which is dependent only on the z component of the magnetic field. We also consider a simple tissue model composed of an air-muscle half-space where the transmitter is placed at $d_1 = 1$ cm above the air-muscle interface. The tissue properties are modeled by assigning a dielectric permittivity ϵ to each layer. The dependence of ϵ with frequency is modeled by the 4-term Cole-Cole relaxation model [10] in the same manner as [6].

1) Coupling Parameter: The coupling parameter of a source can be obtained by writing an expression for its current distribution $M_{1z}(x,y)$ and substituting its Fourier transform $\mathcal{M}_{1z}(k_x,k_y)$ into (18). The point source has the form

$$M_{1z}(x,y) = \delta(x,y). \quad (26)$$

The Fourier transform of the point source is then simply $\mathcal{M}_{1z}(k_x,k_y) = 4\pi^2$. Similarly, the uniform source is modeled as a circle function with a fixed radius R,

$$M_{1z}(x,y) = \begin{cases} 1 & \text{if } \sqrt{x^2+y^2} < R \\ 0 & \text{otherwise} \end{cases}. \quad (27)$$

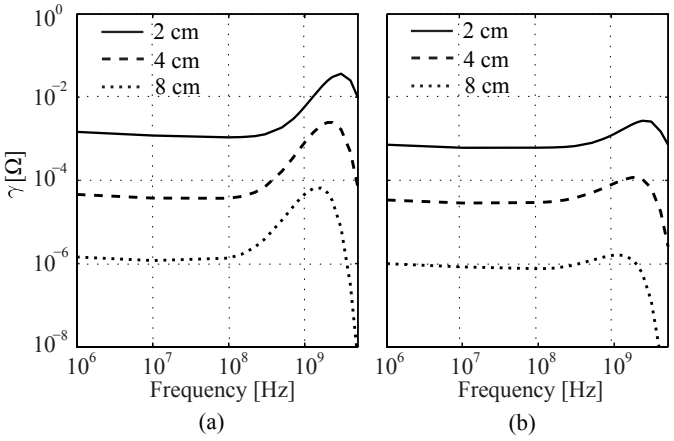

Figure 4. The coupling parameter γ versus frequency for a vertical magnetic dipole receiver at depths $z_f - d_1 = 2$ cm, 4 cm, and 8 cm for (a) the optimized current distribution and (b) a uniform source.

The Fourier transform of the circle function is given by

$$\mathcal{M}_{1z}(k_x, k_y) = \frac{2\pi R J_1(R\sqrt{k_x^2 + k_y^2})}{\sqrt{k_x^2 + k_y^2}} \tag{28}$$

where J_1 is a Bessel function of the first kind and of the first order. For the uniform source, we choose a radius $R = 1$ cm. Further increasing the size of the uniform source actually reduces the coupling parameter due to increased tissue loss.

Fig. 3 shows the coupling parameter versus frequency of each source for an implant at $z_f = 5$ cm. At low frequencies (<100 MHz), the improvement of the optimal source coupling over the point and uniform sources is negligible. At higher frequencies, however, the gain obtained by optimization is significant. For example, at 2 GHz, the optimal source outperforms the point source and the uniform source by about 11 dB. Although the uniform source covers a larger area than point source, its coupling parameter is only slightly higher since the current distribution over the area has not been optimized.

The coupling parameter versus frequency at three different depths in tissue is shown in Fig. 4 for the optimal and the uniform source. The coupling parameter drops with depth much more quickly for the uniform source than the optimized source. This suggests that the gain obtained by transmitter optimization increases with the depth of the implant.

2) Field Distributions: For a given transmitter, the $\mathbf{E}$ and $\mathbf{H}$ fields can be computed everywhere in tissue. The magnitude of the $\mathbf{E}$ field is responsible for tissue heating while, for the vertical magnetic dipole, power is delivered by the z-component of the $\mathbf{H}$ field. The absorbed power in tissue is measured by the specific absorption rate (SAR), which is defined as the absorbed power spatially averaged over a volume of 1 cm^3. The IEEE safety guidelines require that the SAR not exceed 1.6 mW/cm^3 [11].

Fig. 5 shows the distribution of the received open-circuit voltage and SAR distribution at 2 GHz for the uniform and optimal sources. The open-circuit voltage distribution represents the emf induced in a receiver located at a given position. As a basis of comparison between sources, the

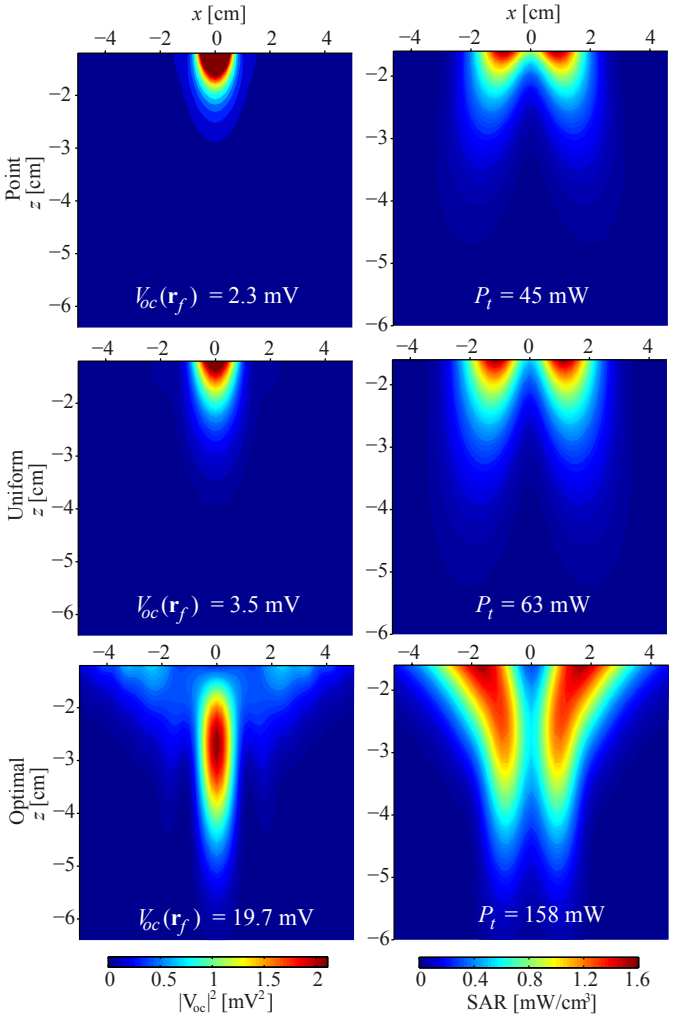

Figure 5. The distribution of V_{oc} and SAR at $y = 0$ in the tissue for the point, uniform, and optimal sources at 2 GHz. The receiver is a magnetic dipole with normal oriented along the z direction, and $(d_1, z_f) = (1$ cm, 5 cm).

transmit power is normalized such that the peak SAR is equal to the safety guideline for each source. The field distributions of the point source and uniform source are highly similar. However, the fields due to the optimal source exhibit *focusing*, the effect where the fields are redistributed such that they interfere constructively at the focal point and destructively otherwise. This enables the optimized source to achieve a 11 dB improvement as compared to the uniform source.

B. Optimal Transmit Distribution

Using the same tissue model, we consider the optimal current distribution for both a magnetic and electric dipole. The magnetic dipole is again oriented in the z direction with area $A_r = \pi$ mm^2. The electric dipole is lying parallel to the x direction with length $l_r = 2$ mm.

For the magnetic dipole receiver, the optimal current distribution $M_{1z,opt}$ is circularly symmetric. Fig. 6 shows the magnitude and phase of a radial slice of $M_{1z,opt}$ at 2 MHz and 2 GHz for an implant at $z_f = 5$ cm. At both frequencies, the magnitude decays quickly and is negligible at large radial distances. At low frequencies, the magnitude is negligible

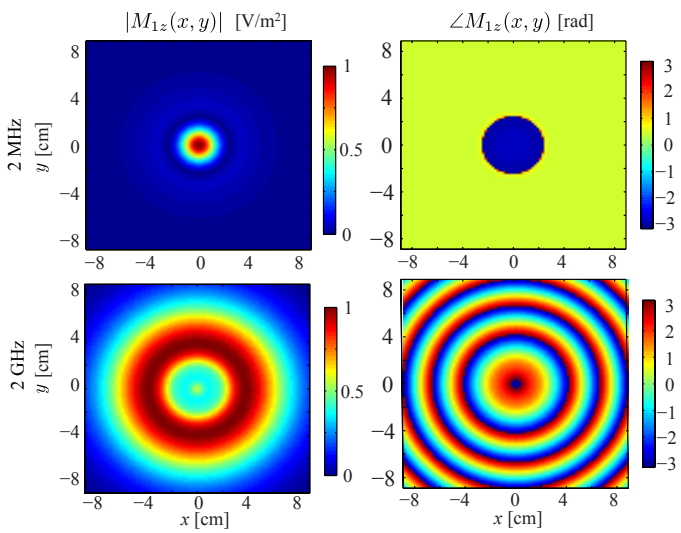

Figure 6. Magnitude and phase of $M_{1z,opt}(x,y)$ at 2 MHz and 2 GHz for the receive mangetic dipole where $(d_1, z_f) = (1 \text{ cm}, 5 \text{ cm})$.

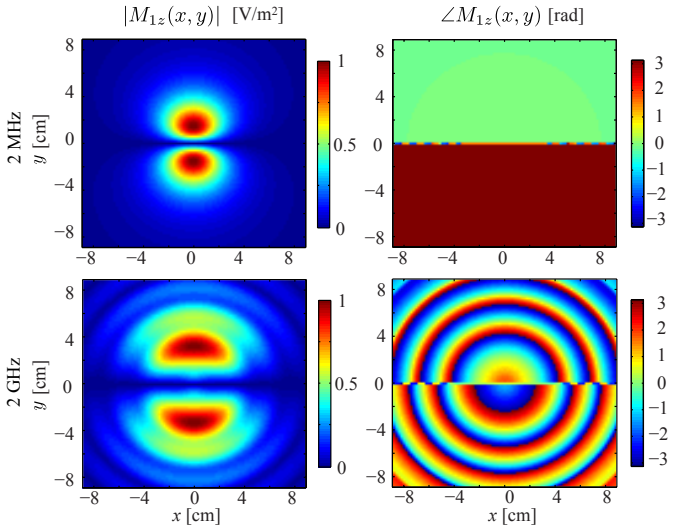

Figure 7. Magnitude and phase of $M_{1z,opt}(x,y)$ at 2 MHz and 2 GHz for the receive electric dipole where $(d_1, z_f) = (1 \text{ cm}, 5 \text{ cm})$.

outside $\rho = 2$ cm while the phase is almost constant within the circular region. Due to the relatively long wavelengths in tissue, there are no interference effects and optimal source is obtained by placing all of the energy at the point closest to the receiver. At high frequencies, however, the magnitude of the optimal current distribution extends a much larger radius and the phase varies quickly with a period of wavelength in tissue. The distribution resembles a ring and leads to constructive interference at the implant and destructive interference elsewhere.

For a receive electric dipole, the optimal current distribution is *not* circularly symmetrical. Since the transmitter is composed of magnetic dipoles, circularly symmetric sources, such as the point and uniform source, result in zero $\mathbf{E}$ field along the z-axis so no power is delivered to an electric dipole receiver. Instead, Fig. 7 shows that the distribution is conjugate symmetric across the x-axis such that the $\mathbf{E}$ fields add constructively along the direction of the dipole in x. The current distribution also exhibits decaying behavior similar to the magnetic dipole at both frequencies.

The optimal transmit current distribution was found along an infinite sheet. In practice, the transmitter can be realized only within a limited area. An important property of the optimal current distribution is that the magnitude decays rapidly as the radial distance ρ increases, as shown in both Fig. 6 and 7. Since the contribution of the current becomes negligible at large radial distances, an optimal transmitter dimension can be defined for which beyond there is a diminishing return in performance. The ν-radius of the transmitter is defined as the radius ρ_ν where

$$\int_{\sqrt{x^2+y^2}\leq\rho_\nu} \left|M_{z,opt}(x,y)\right|^2 dxdy = \nu \int \left|M_{z,opt}(x,y)\right|^2 dxdy \tag{29}$$

for $0 < \nu \leq 1$. For example, $\rho_{0.9}$ gives the radius of the transmit current distribution that it contains 90% energy of in the optimal source distribution. The current outside the ν-radius can be safely ignored with minimal impact on the coupling parameter [7].

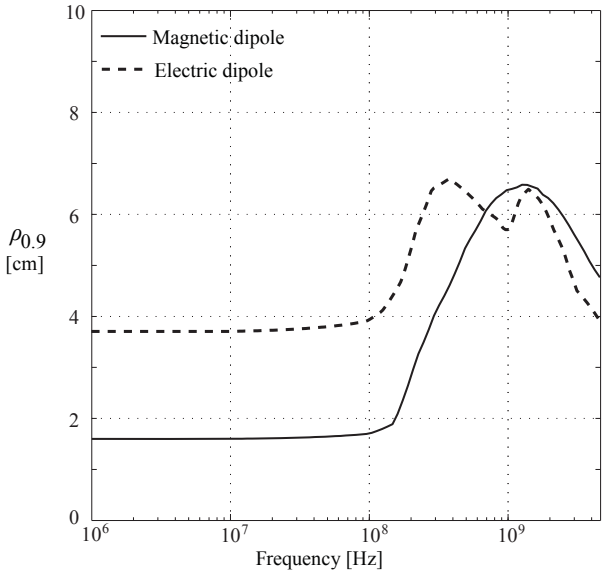

Figure 8. $\rho_{0.9}$ versus frequency for a magnetic dipole and electric dipole receiver at depth $z_f - d_1 = 4$ cm.

Fig. 8 shows $\rho_{0.9}$ for a receiving magnetic and electric dipole at $z_f = 5$ cm. Somewhat counterintuitively, the ν-radius is small for low frequencies, which suggests that in this range the optimal current distribution resembles a small uniform source. This is consistent with the results in Fig. 3 where the uniform and optimal sources were found to have comparable performance at low frequencies. The ν-radius then increases with frequency up to the low GHz range, beyond which it decreases again due the excessive tissue loss past the low-GHz range. Fig. 9 shows $\rho_{0.9}$ with varying depths of a magnetic dipole receiver. The ν-radius increases with the depth of the implant.

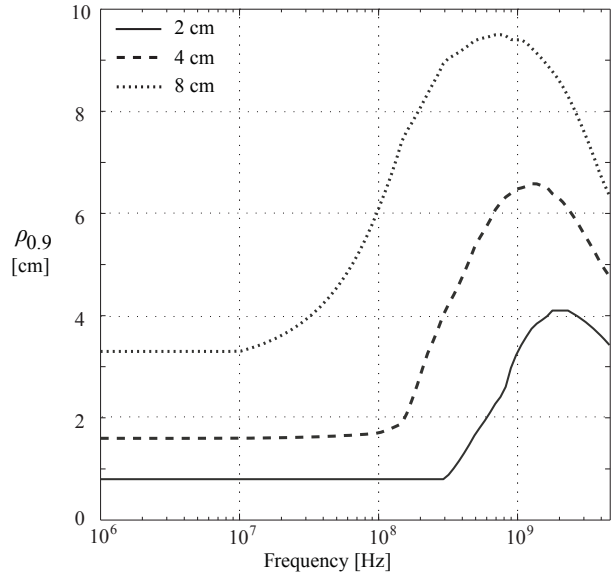

Figure 9. $\rho_{0.9}$ versus frequency for a magnetic dipole receiver at depths $z_f - d_1 = 2$ cm, 4 cm, and 8 cm.

VI. Receiver Considerations

Optimizing the transmit current distribution allows the maximum coupling parameter γ_{opt} to be obtained, and hence the maximum coupling efficiency $\eta_{c,opt} = \gamma_{opt}/4R_{22}$ as well for a given receiver. The total power transfer efficiency, however, is given by the product of the coupling efficiency η_c and the matching efficiency η_m. In this section, we show how the matching efficiency can be maximized subject to practical limitations that arise in an integrated circuit (IC) implementation of the receiver [12], [13]. This establishes an upper-bound on the power transfer efficiency that can be obtained for a given receiver in tissue.

From (5), the matching efficiency is given by

$$\eta_m = \frac{4R_{22}R_L}{\left|Z_{22} + Z_L\right|^2} \tag{30}$$

where Z_{22} is the self-impedance of the receiving antenna and Z_L is the load impedance. For a fixed frequency, Z_{22} is determined by the antenna dimensions and material as well as the surrounding tissue. The load impedance Z_L, however, can be controlled by introducing a *matching network* between antenna and the load as shown in Fig. 2. Note that the *conjugate matching* condition

$$Z_L = Z_{22}^* \tag{31}$$

yields the maximum matching efficiency $\eta_m = 1$. Conjugate matching requires both *resonance*, which occurs when the imaginary part of Z_L cancels that of Z_{22}, and *matched resistance*, the condition where $R_L = R_{22}$.

Practical limitations to conjugate matching arise from the limited transformation range of the matching network. Supposing that the resonance condition is met, the matching network must be able to perform impedance transformation between the antenna and the load in order to achieve matched resistance. For typical implants, the load impedance is determined by the rectifier, which has values on the order of 1 kΩ [12], [13]. On an IC, however, the Q-factor is typically limited to <10, which yields a maximum transformation ratio of 1:100. As such, we have the minimum load resistance condition

$$R_L > 10\ \Omega. \tag{32}$$

This limits our ability to perform conjugate matching when the antenna self-resistance is small.

Table I
Optimal power transfer efficiency for typical values of R_{22} and minimum load resistance $R_L = 10\,\Omega$

Receiver	Frequency [MHz]	R_{22} [Ω]	γ_{opt} [dB(Ω)]	$\eta_{c,opt}$ [dB]	η_m [dB]	η_{opt} [dB]
Magnetic dipole	2	0.02	−43.8	−32.8	−21.0	−53.8
	20	0.02	−44.4	−33.4	−21.0	−54.4
	200	0.08	−43.2	−38.3	−15.0	−53.3
	2000	10.6	−26.1	−42.4	0	−42.4
Electric dipole	2	1307	−23.4	−60.6	0	−60.6
	20	1105	−24.1	−60.6	0	−60.6
	200	546	−23.3	−56.7	0	−56.7
	2000	29	−17.5	−38.1	0	−38.2

Table I lists the optimal power transfer efficiency for different frequencies. The values of R_{22} were obtained for a magnetic dipole of radius 1 mm and an electric dipole of length 2 mm in muscle, and are typical of the antenna self-impedance. Interestingly, R_{22} of electric dipole is high at low frequencies, which is opposite of the result in free space. This is due to the high dielectric loss around the dipole in a lossy medium. For the magnetic dipole, conjugate matching cannot be achieved at low frequencies due to small values of R_{22}.

When receiver considerations are taken into account, Table I shows that the optimal frequency remains in the low-GHz range. Although the optimal coupling parameter γ_{opt} of the electric dipole is much higher than the magnetic dipole, the power transfer efficiency is somewhat worse due to high dielectric loss in the surrounding tissue. Since matching efficiency is independent of transmit source, the effect of the receiver considerations will be identical for other sources. The gain obtained by optimization of the coupling parameter directly translates to an increase in power transfer efficiency.

VII. Conclusions

We studied the optimal transmitter for wireless power transfer to small receiver embedded in multiple planar layers of tissue. We considered a general transmitter composed of an arbitrary magnetic current sheet, and allowed for a receiver modeled by a combination of magnetic and electric dipoles with arbitrary orientations. On abstracting the coupling between the transmitter and the receiver as a two-port network, an expression for the power transfer efficiency was derived and found to be the product of the coupling and matching efficiency. We expressed the coupling efficiency in terms of the fields in tissue via a plane wave decomposition and derived the magnetic current distribution that maximizes the coupling efficiency for a given receiver. The optimal source was then compared to the point and uniform source. Finally, receiver

considerations were taken into account to find the improvement in power transfer efficiency obtained by transmitter optimization.

The optimal source distribution achieves the highest power transfer efficiency at the low-GHz range. At the low-GHz range, we found that the optimal source distribution does not resemble the uniform distribution, but is more complicated in shape. Consequently, the optimal source invokes focusing of electromagnetic fields to concentrate fields at the receive implant while reducing of the heating in the surrounding tissue, which results in substantial improvement in the power transfer efficiency. Lastly, the optimal source distribution informs us a dimension of the transmit antenna beyond which there is a diminishing return in performance.

ACKNOWLEDGEMENT

The authors would like to thank Hang Wong of the City University of Hong Kong for the useful discussions and valuable comments. In addition, the authors acknowledge the support of the C2S2 Focus Center, one of six research centers funded under the Focus Center Research Program (FCRP), a Semiconductor Research Corporation entity; and the support from Kwanjeong Educational Foundation.

REFERENCES

[1] I. C. Forster, "Theoretical design and implementation of a transcutaneous, multichannel stimulator for neural prosthesis applications," *J. Biomed. Engng.*, vol. 3, pp. 107–120, Apr. 1981.

[2] N. N. Donaldson and T. Perkins, "Analysis of resonant coupled coils in the design of radio frequency transcutaneous links," *Med. Biol. Eng. Comput.*, vol. 21, pp. 612–627, Sep 1983.

[3] E. S. Hochmair, "System optimization for improved accuracy in transcutaneous signal and power transmission," *IEEE Trans. Biomed. Eng.*, vol. 31, pp. 177–186, Feb. 1984.

[4] U. Jow and M. Ghovanloo, "Design and optimization of printed spiral coils for efficient transcutaneous inductive power transmission," *IEEE Trans. Biomed. Circuits Syst.*, vol. 1, pp. 193–202, Sep. 2007.

[5] A. RamRakhyani, S. Mirabbasi, and M. Chiao, "Design and optimization of resonance-based efficient wireless power delivery systems for biomedical implants," *IEEE*, vol. 5, pp. 48 –63, Feb. 2011.

[6] A. S. Y. Poon, S. O'Driscoll, and T. H. Meng, "Optimal frequency for wireless power transmission into dispersive tissue," *IEEE Trans. Antennas And Propagation*, vol. 58, pp. 1739–1750, May 2010.

[7] S. Kim and A. S. Y. Poon, "Optimal transmit dimension for wireless powering of miniature implants." Antennas and Propagation Society International Symposium (APSURSI), July 2011.

[8] R. F. Harrington, *Time-Harmonic Electromagnetic Fields*. IEEE Press, 2001. ch. 3.

[9] W. C. Chew, *Waves and Fields in Inhomogeneous Media*. IEEE Press, 1995.

[10] S. Gabriel, R. W. Lau, and C. Gabriel, "The dielectric properties of biological tissues: III. Parametric models for the dielectric spectrum of tissues," *Phys. Med. Biol.*, vol. 41, pp. 2271–2293, Nov. 1996.

[11] "IEEE standard for safety with respect to human exposure to radiofrequency electromagnetic fields, 3 kHz to 300 GHz." IEEE Standard C95.1-1999, 1999.

[12] S. O'Driscoll, A. S. Y. Poon, and T. H. Meng, "A mm-sized implantable power receiver with adaptive link compensation," in *Proc. IEEE Intl. Solid-State Circuits Conf. (ISSCC)*, Feb. 2009.

[13] A. Yakovlev, D. Pivonka, T. H. Meng, and A. S. Y. Poon, "A mm-sized wirelessly powered and remotely controlled locomotive implantable device," in *Proc. IEEE Intl. Solid-State Circuits Conf. (ISSCC)*, Feb. 2012.

Sanghoek Kim (S'09) received his B.S. degree with a double major in electrical engineering and mathematics from Seoul National University in 2007. He received the M.S. degree in Electrical Engineering from Stanford University in 2009, where he is currently working toward a Ph.D. degree. His research interests include wireless power transfer, and biomedical applications of radio-frequency technology. He is a recipient of the Kwanjeong Educational Foundation Scholarship.

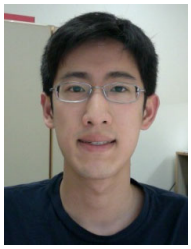

John. S. Ho (S'11) was born in California. He received the B.Eng degree in Electronic and Computer Engineering at the Hong Kong University of Science and Technology (HKUST) and is currently pursuing his M.S. and Ph.D degrees in Electrical Engineering at Stanford University.

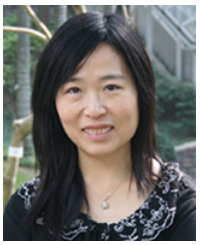

Ada S. Y. Poon (S'98–M'04–SM'10) was born in Hong Kong. She received the B.Eng and M.Phil. degrees in Electrical and Electronic Engineering from the University of Hong Kong, and received the M.S. and Ph.D. degrees in Electrical Engineering and Computer Sciences from the University of California at Berkeley.

In 2004, she was a senior research scientist at Intel Corporation, Santa Clara, CA. In 2005, she was a senior technical fellow at SiBeam, Inc., Fremont, CA. In 2006–2007, she was an assistant professor at the Department of Electrical and Computer Engineering in the University of Illinois at Urbana-Champaign. Since 2008, she has been at the Department of Electrical Engineering in Stanford University, where she is currently an assistant professor. Her research focuses on applications of wireless communication and integrated circuit technologies to biomedicine and health care.